Electronic Supplementary Material (ESI) for Journal of Materials Chemistry A.

Ultra-stretchable and Multifunctional Wearable Electronics for Superior Electromagnetic Interference Shielding, Electrical Therapy and Biomotion Monitoring

Wei Zhai,[a] Chunfeng Wang,[b] Shuo Wang,[a] Jiannan Li,[a] Yi Zhao,[a] Pengfei Zhan,[a] Kun Dai,[a]* Guoqiang Zheng,[a] Chuntai Liu,[a]* and Changyu Shen[a]

[a] *Key Laboratory of Materials Processing and Mold (Zhengzhou University), Ministry of Education, School of Materials Science and Engineering, Zhengzhou University, Zhengzhou, Henan 450001, P. R. China*

[b]*College of Physics and Optoelectronic Engineering, Shenzhen University, Shenzhen 518060, P. R. China*

* Correspondence author:

E-mail: kundai@zzu.edu.cn (K. Dai), ctliu@zzu.edu.cn (C. L.)

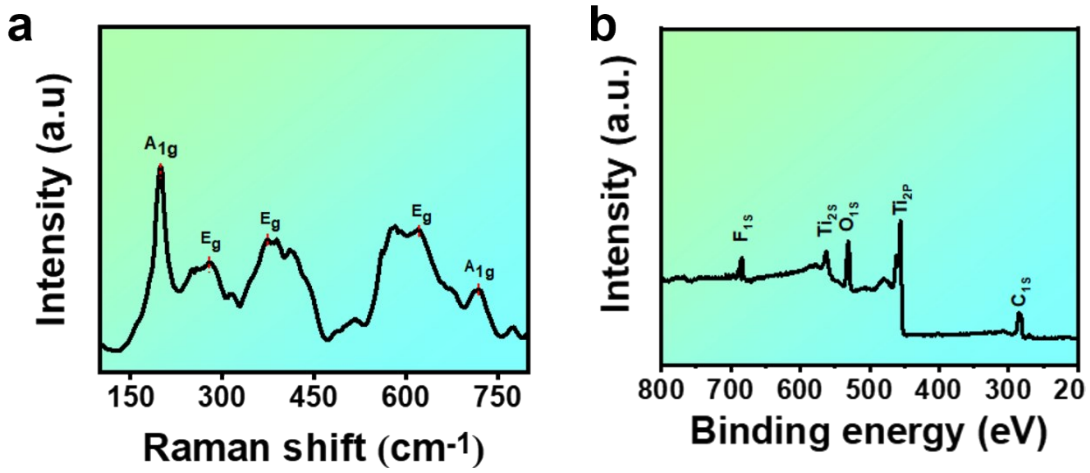

Fig. S1. Raman spectrum and XPS of MXene.

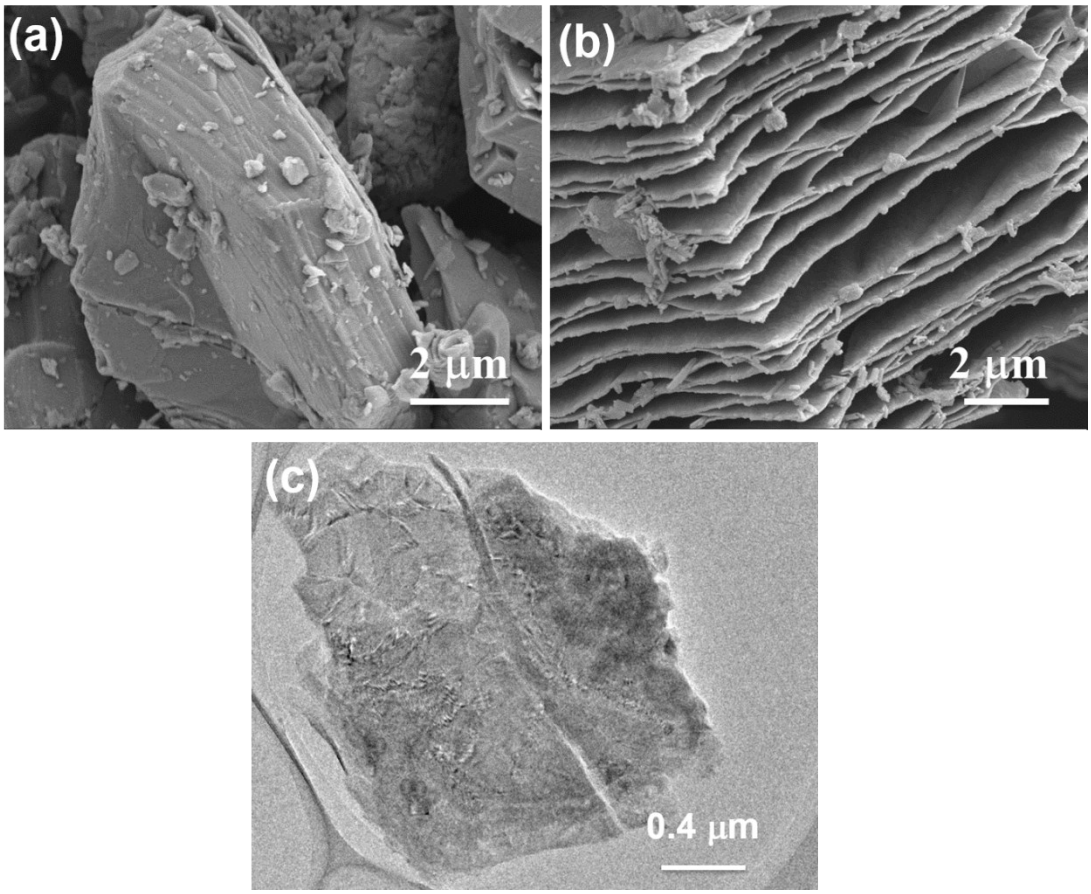

Fig. S2. SEM image of Max (a) and MXene (b); and TEM image of MXene nanosheets (c).

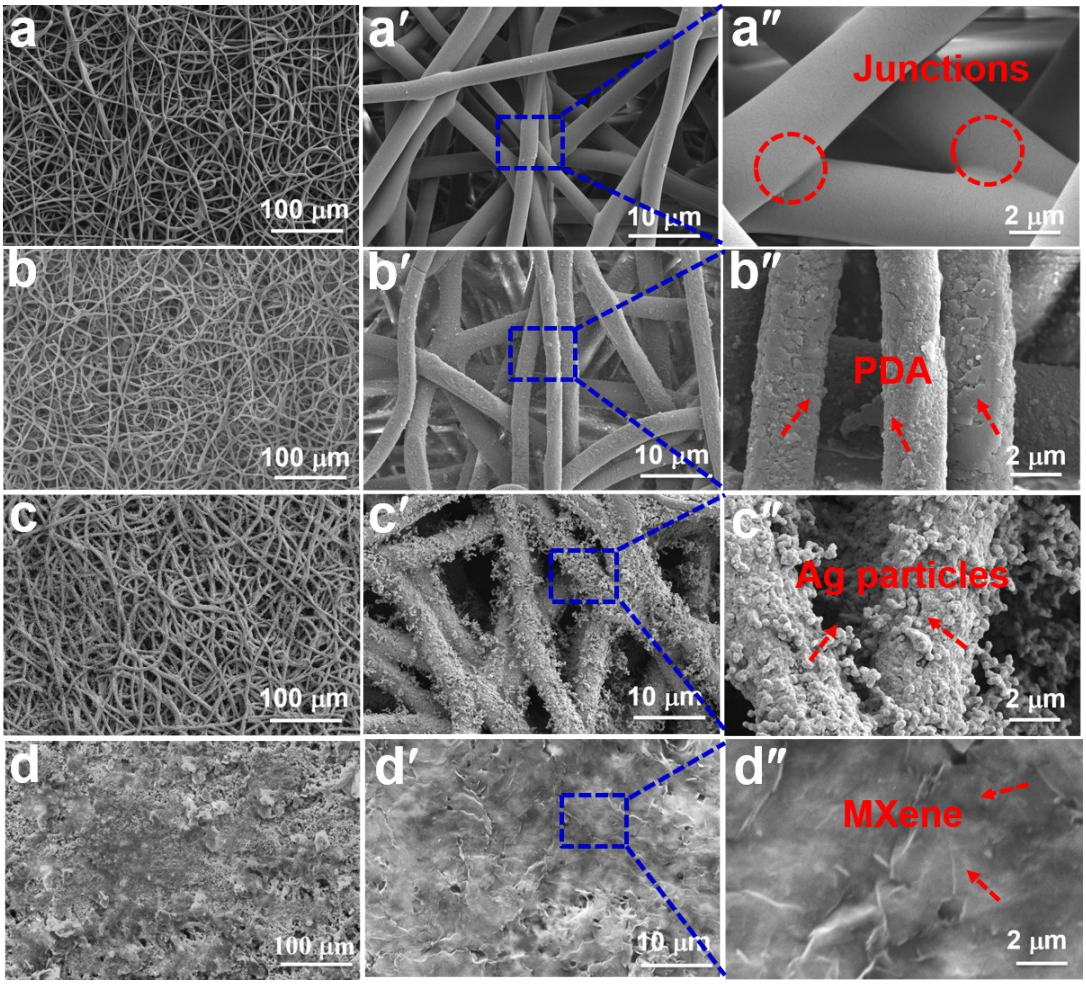

Fig. S3. SEM images of neat TPU fibrous film (a-a″), TPU/PDA fibrous film (b-b″), TPU/PDA/AgNPs fibrous film (c-c″) and TPU/PDA/AgNPs/MXene film (d-d″).

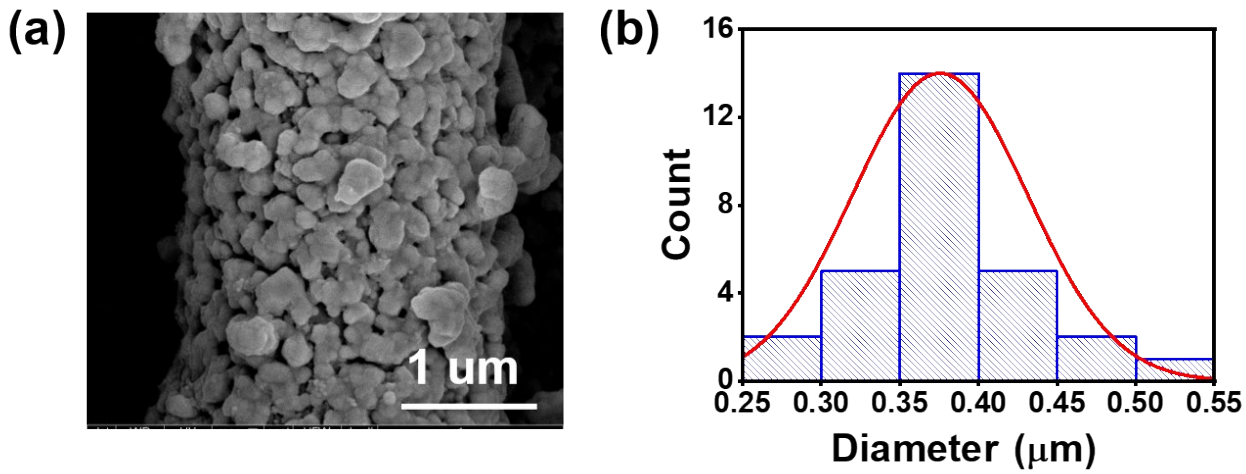

Fig.S4 Morphology and diameter of AgNPs in TAF.

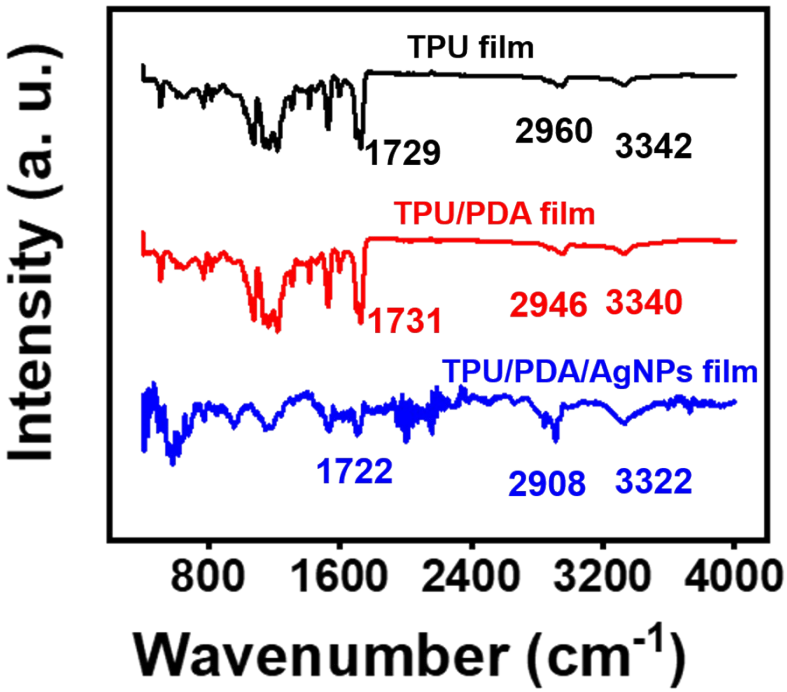

Fig. S5. FTIR spectra of pure TPU, TPU/PDA and TPU/PDA/AgNPs film.

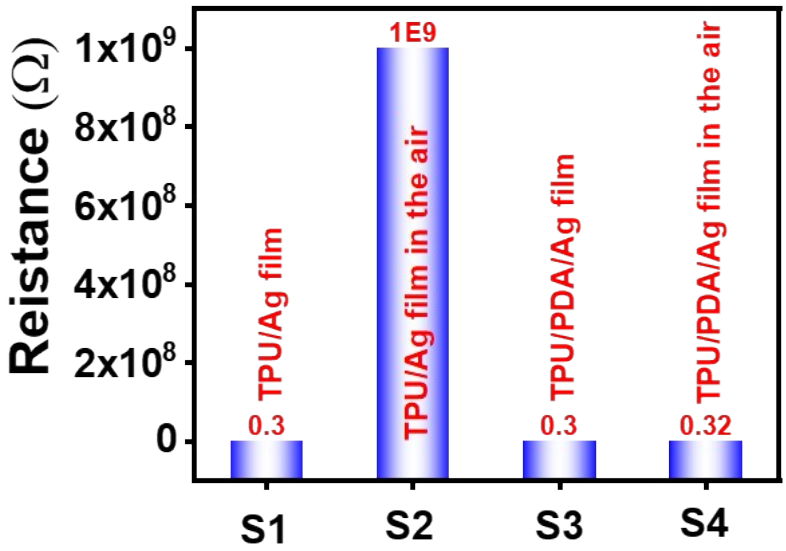

Fig. S6. Influence of the introduction of PDA on the conductivity of TPU/AgNPs film.

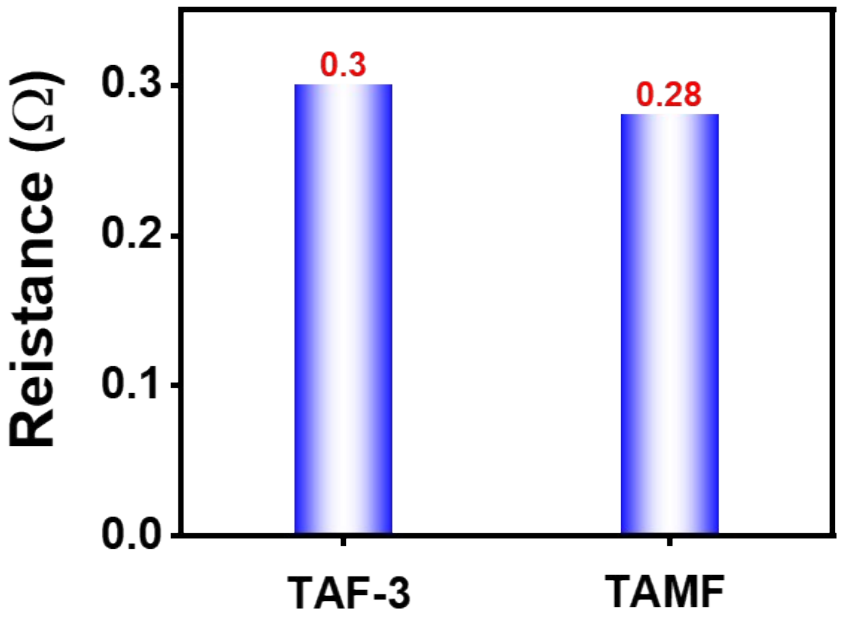

Fig. S7. The effect of the introduction of MXene nanosheets on the resistance.

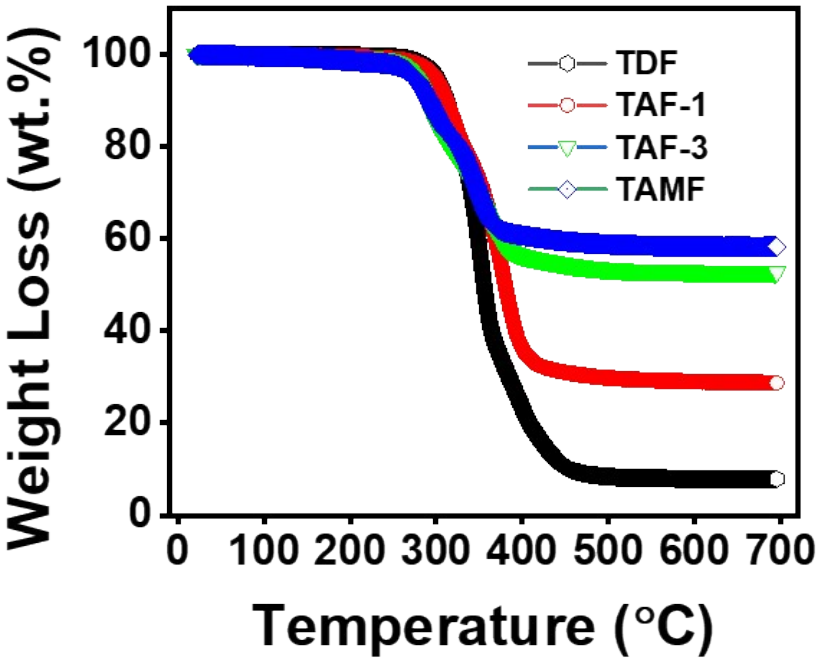

Fig.S8 Thermogravimetric analysis of TDF, TAF-1, TAF-3 and TAMF.

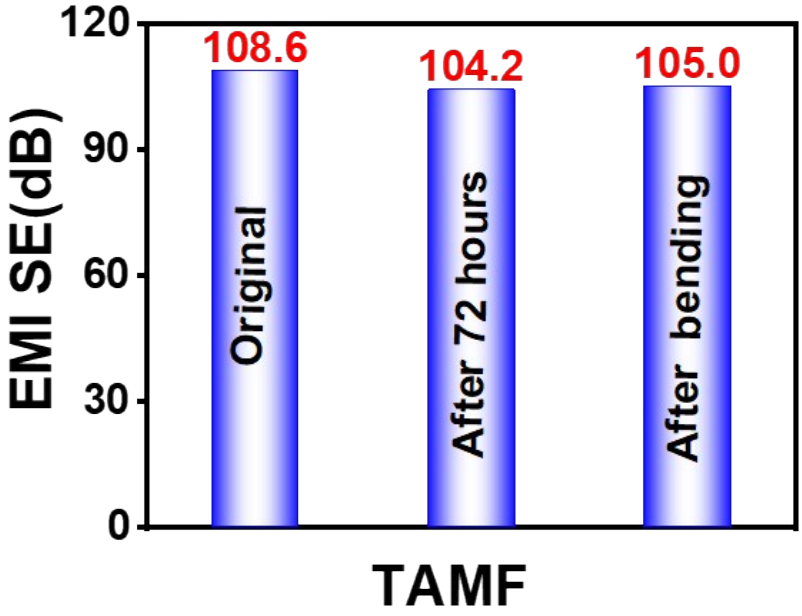

Fig. S9. The EMI SE of TAMF at the initial state, exposure to air for 72 h and underwent 1000 bending-releasing cycle treatments.

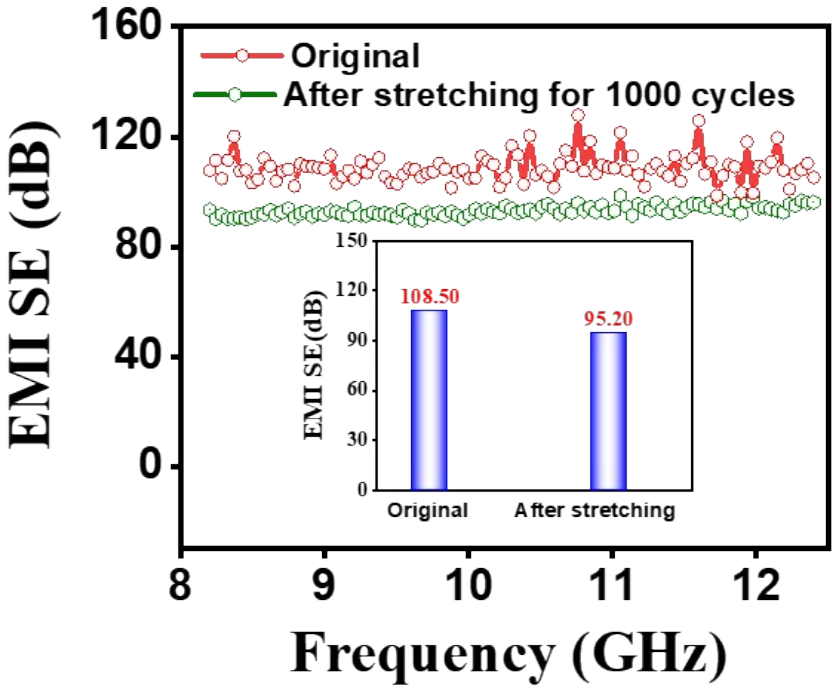

Fig. S10 EMI SE of TAMF before and after 1000 stretching-releasing cycles. The inset shows the corresponding average value.

Table S1 Comparison of EMI shielding performance, conductivity and filler content of our work with previous reports.

Fillers	Content	Conductivity (S/m)	EMI SE	References
MXene	50 wt.%	621	40	Ref.1
AgNWs	3 wt.%	1200	63.9	Ref.2
MXene	100 wt.%	58000	70	Ref.3
Ag@C	100 wt.%	361.1	70	Ref.4
MXene	90 wt.%	26400	50.2	Ref.5
AgNPs	88.5 wt.%	107.2	37.8	Ref.6
MXene/PPy	24 wt.%	1000	90	Ref.7
MXene/rGO	100 wt.%	1000	50.7	Ref.8
AgNPs/MXene	48.4 wt.%	95238	108.6	**This work**

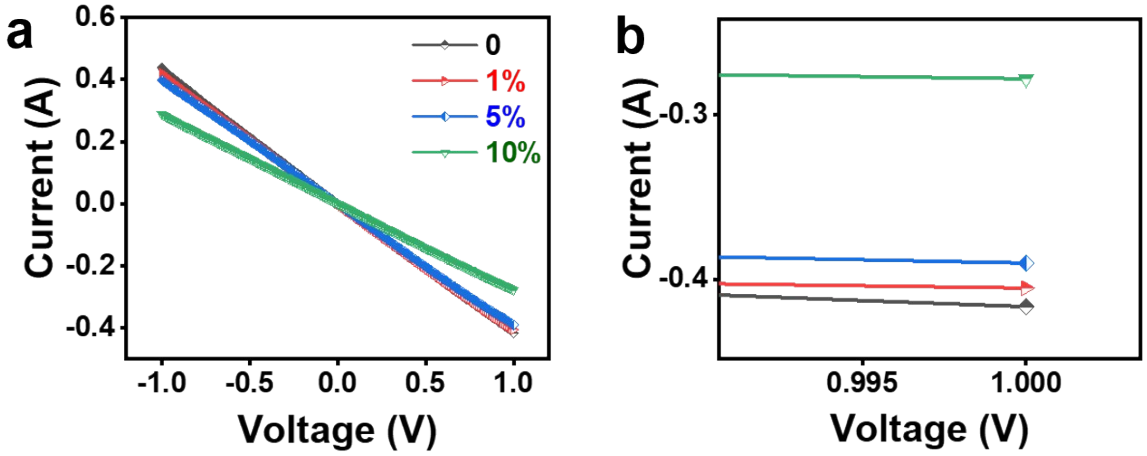

Fig. S11. I-V curves of TAMF in different tensile strain (a), (b) is the magnified view of (a).

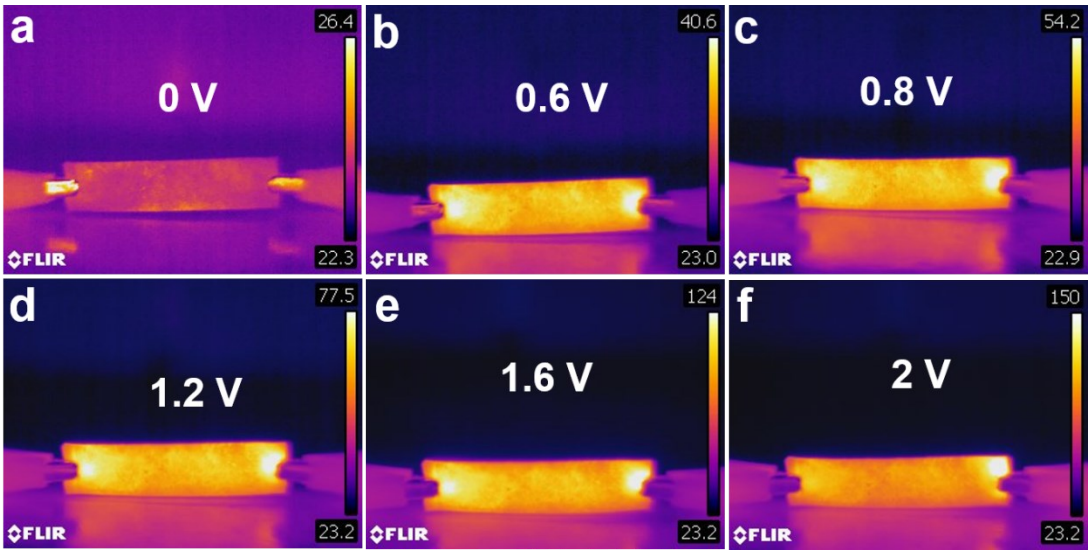

Fig. S12. Digital and IR camera images of the electrical heaters in wearable thermotherapy with supplied voltages of 0, 0.6, 0.8, 1.2, 1.6 and 2.0 V.

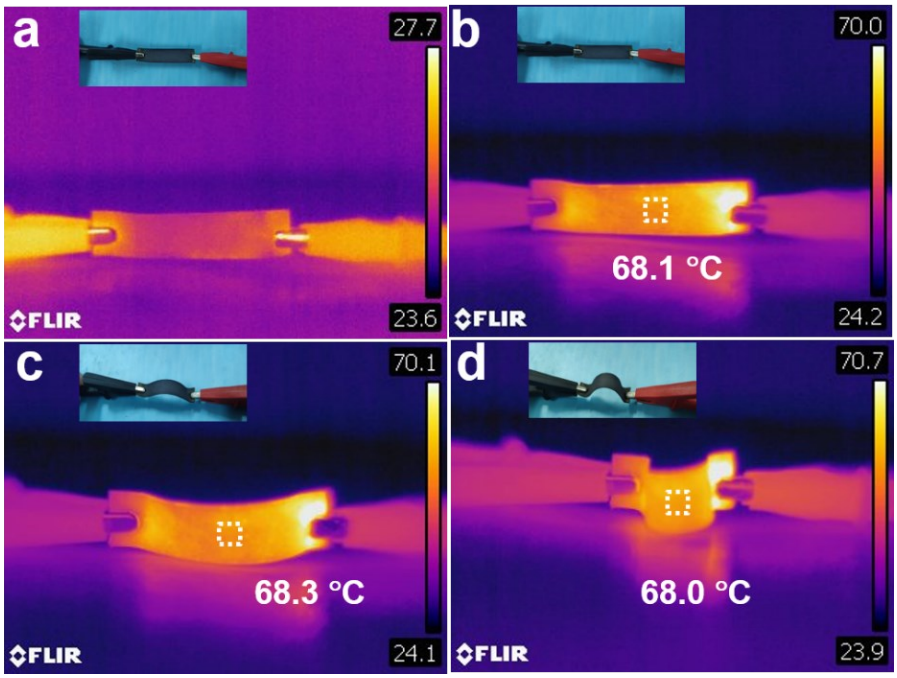

Fig. S13. Digital and IR camera images of the electrical heaters in wearable thermotherapy with different bending angles at the voltage of 0.6 V.

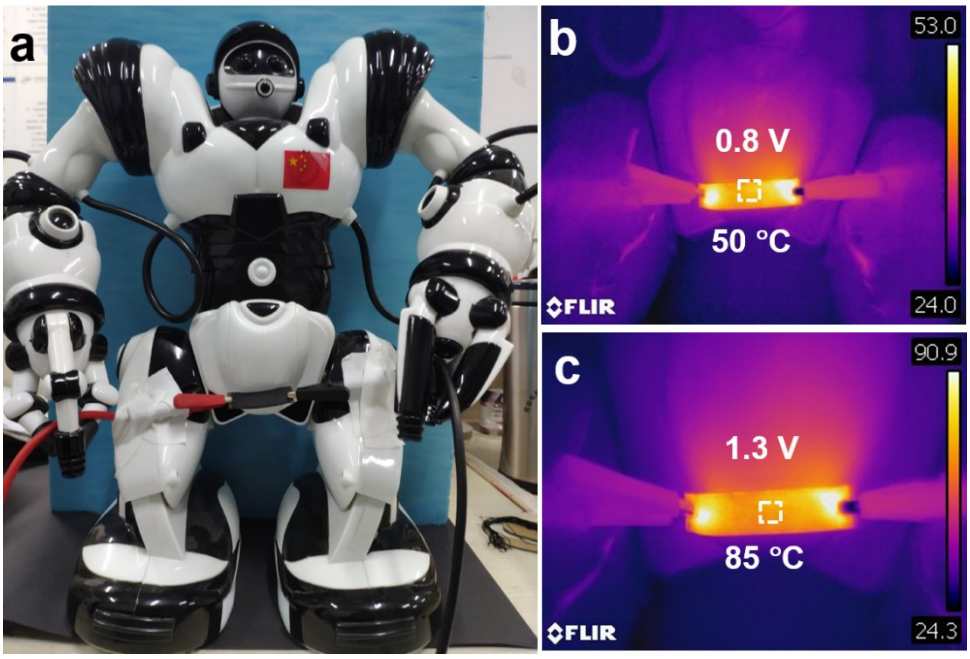

Fig. S14. The TAMF heater is stuck on stomach of a robot and the temperature are tested at the voltage of 0.8V and 1.3 V, respectively.

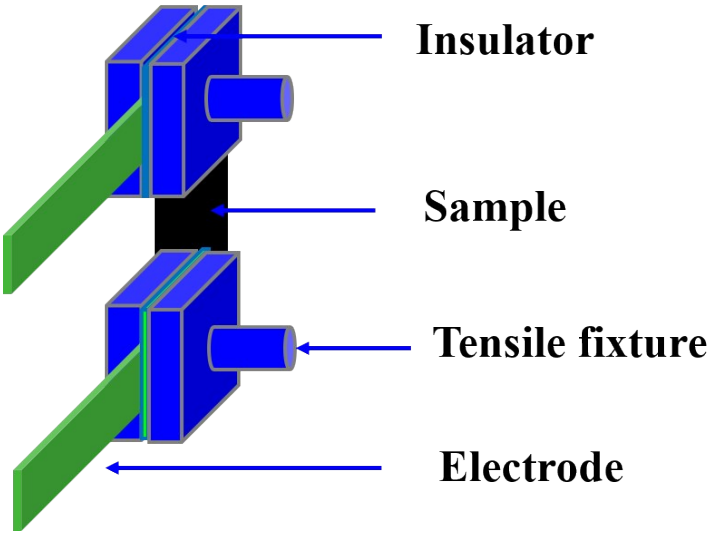

Fig. S15. The schematic of tensile experiment.

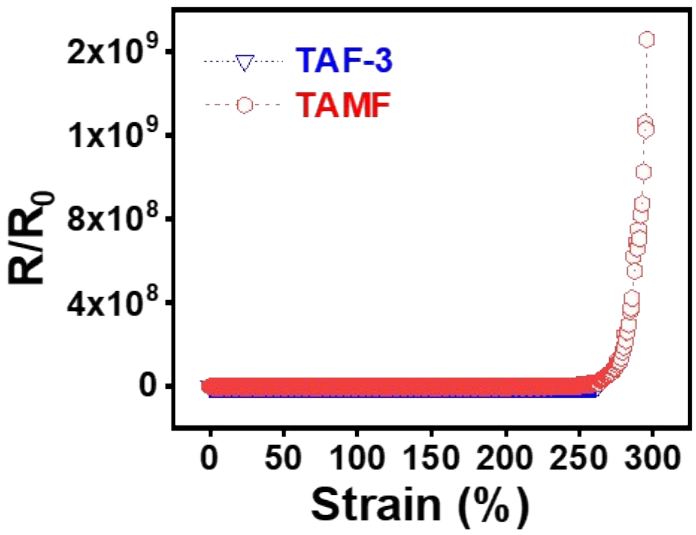

Fig. S16. R/R_0 values of TAF-3 and TAMF as a function of strain.

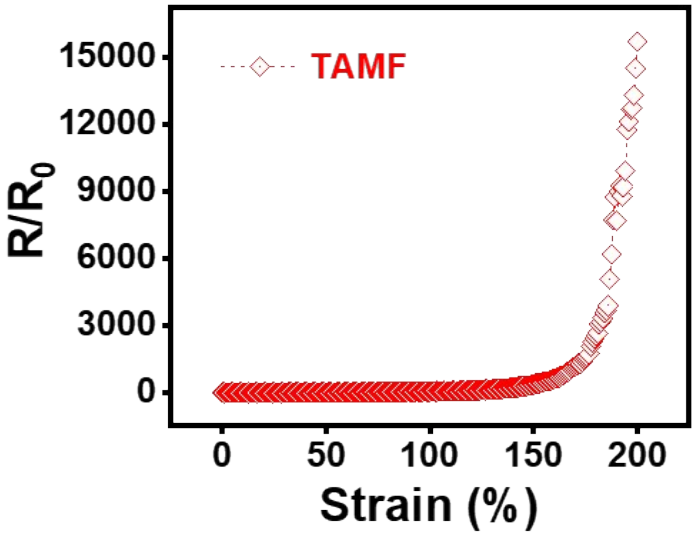

Fig. S17. R/R_0 values of TAMF as a function of strain.

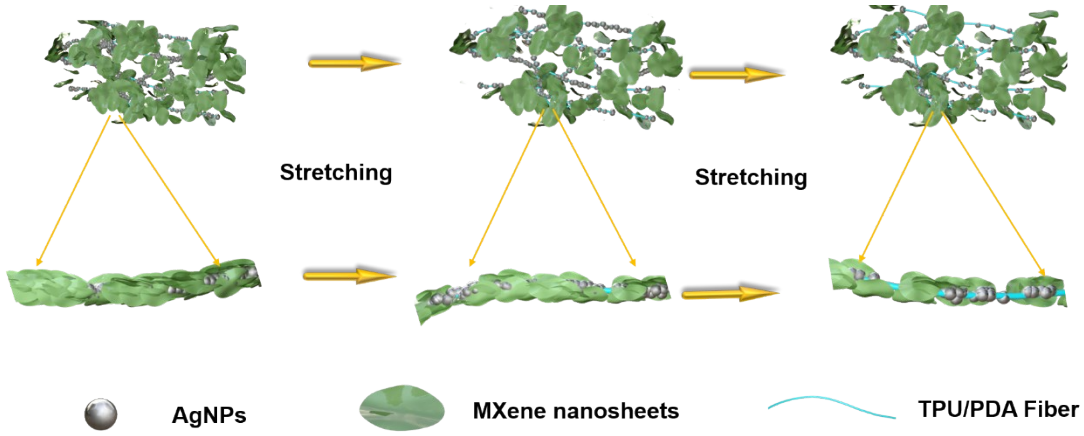

Fig. S18. The strain sensing mechanism of TAMF during stretching.

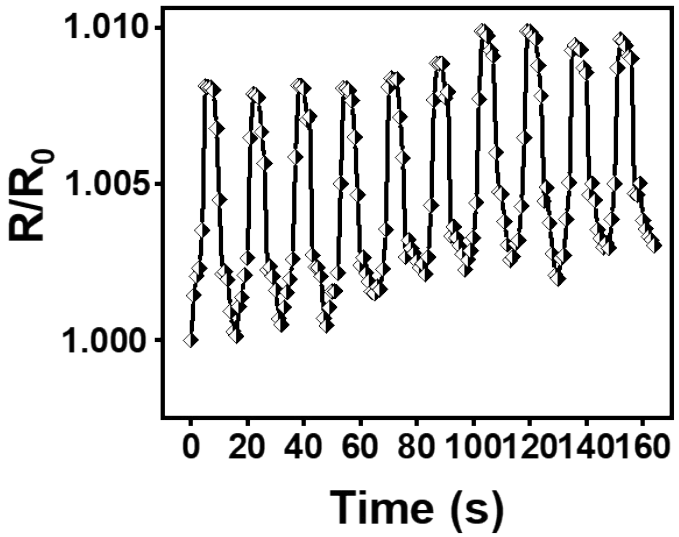

Fig. S19. R/R_0-time curve of TAMF towards the strains of 0.1% in 10 stretching-releasing cycles .

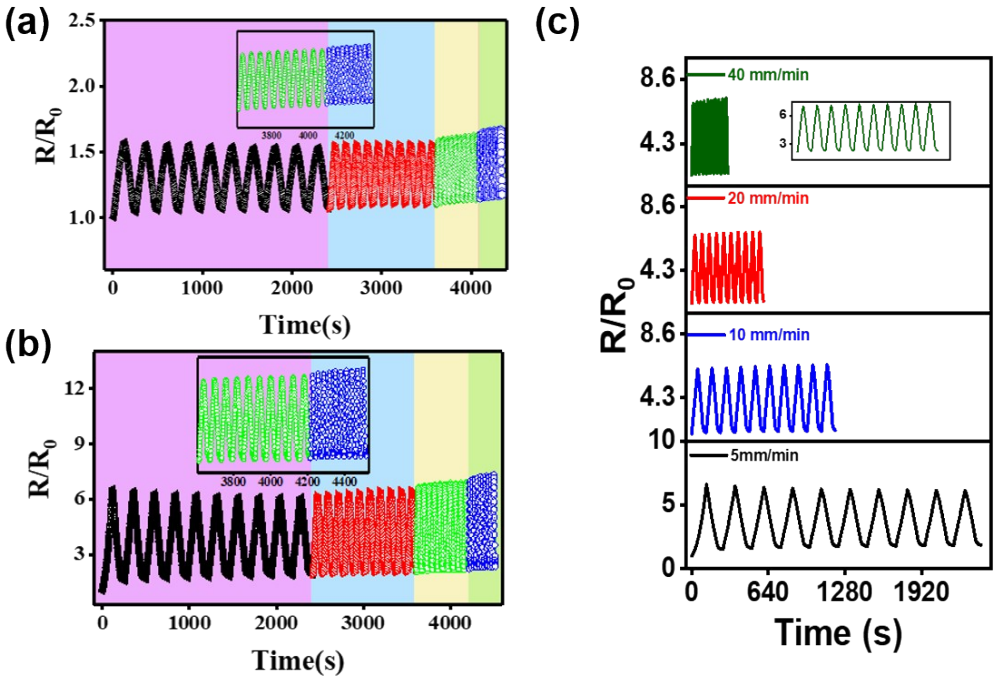

Fig. S20. R/R_0 response of TAMF at varying frequencies under 10% strain (a), 50% strain (b), R/R_0 response of TAMF at different frequencies under 50% strain (c).

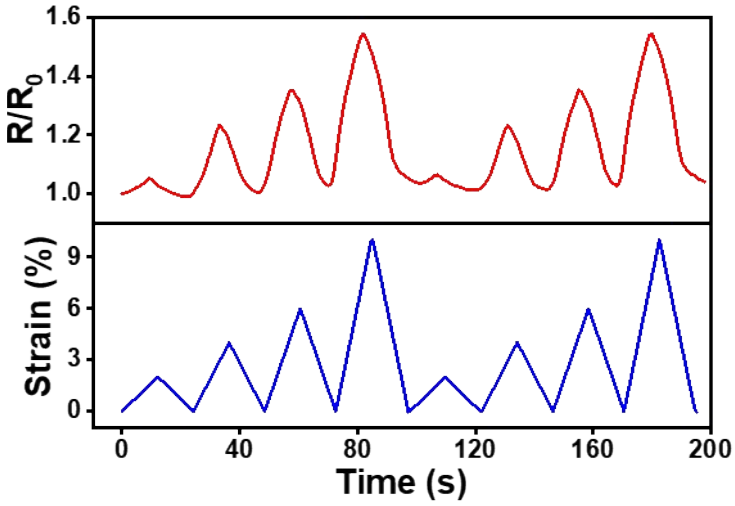

Fig. S21. R/R_0-time and strain-time curves of TAMF with maximum strains of 2%, 4%, 6% and 10% in two stretching-releasing cycles during step cyclic deformation.

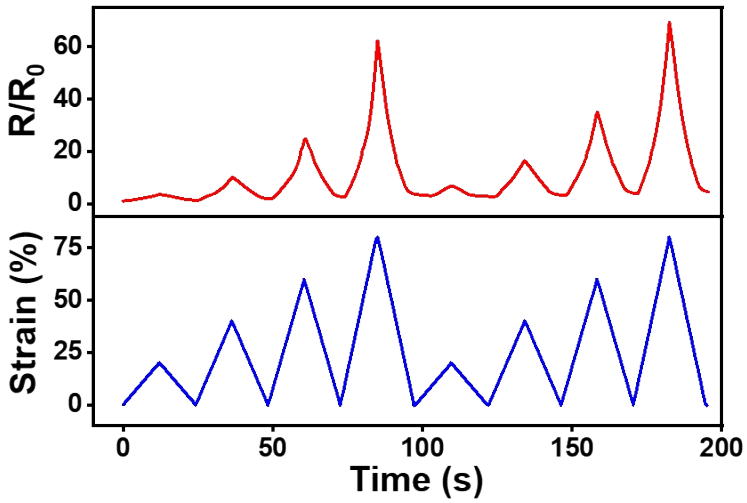

Fig. S22. R/R_0-time and strain-time curves of TAMF with maximum strains of 20%, 40%, 60% and 80% in two stretching-releasing cycles during step cyclic deformation.

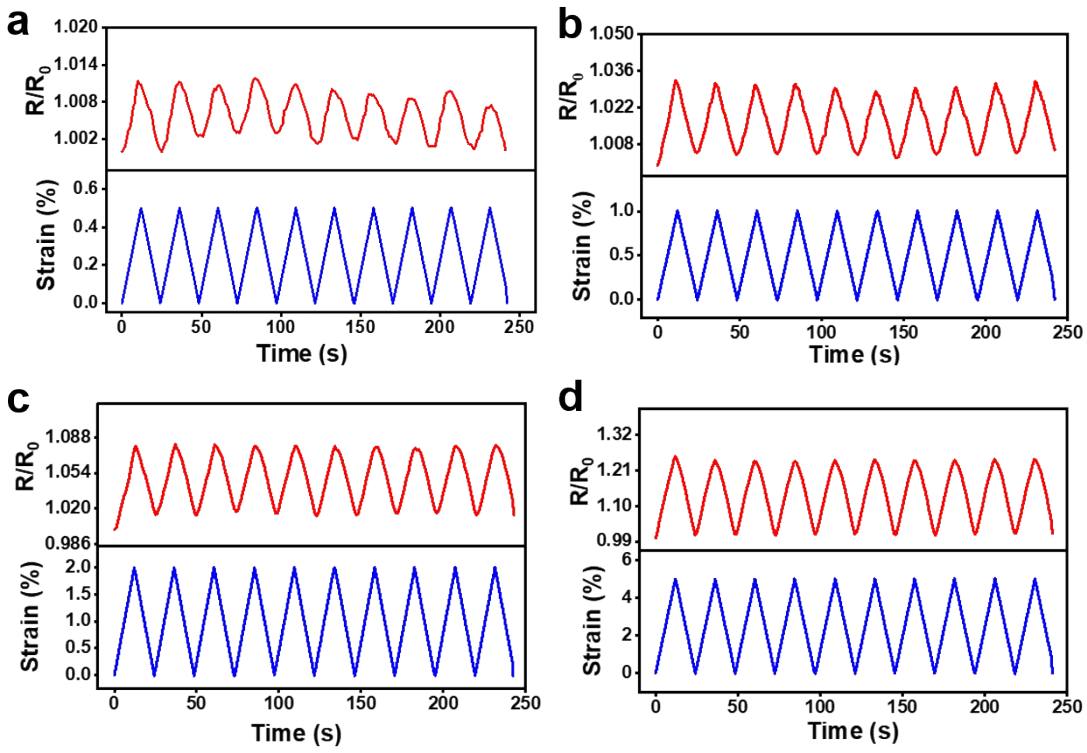

Fig. S23 R/R_0-time and strain-time curves of TAMF with different strains of 0.5% (a), 1% (b), 2% (c) and 5% (d) in 10 stretching-releasing cycles.

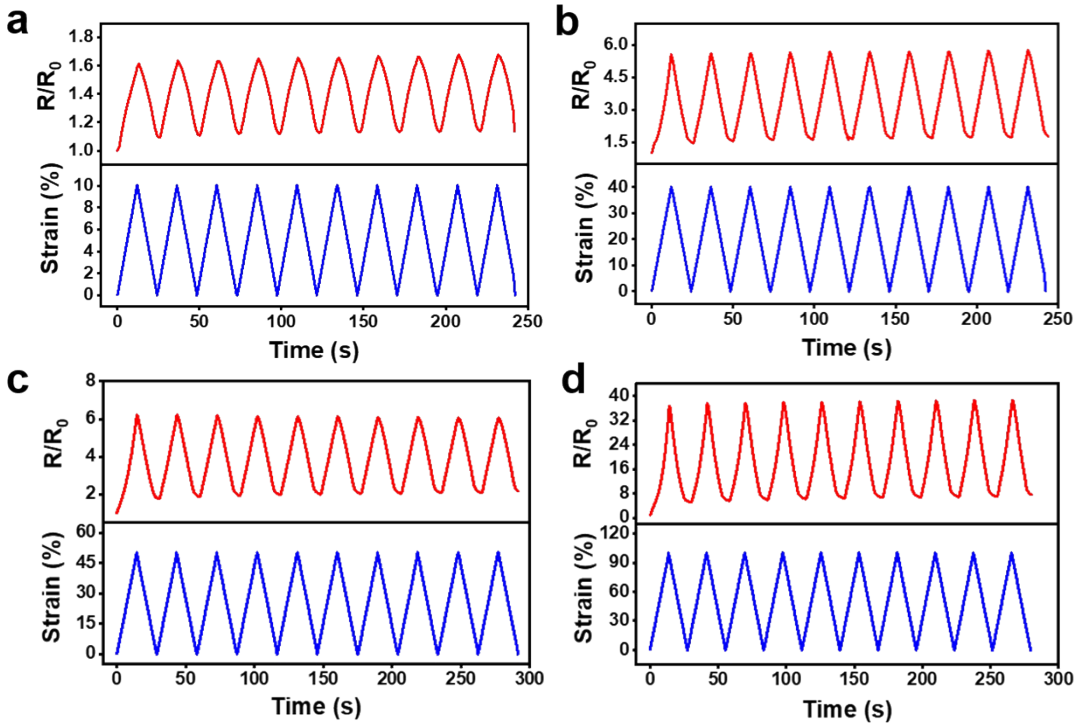

Fig. S24. R/R_0-time and strain-time curves of TAMF with different strains of 10% (a), 40% (b), 50% (c) and 100% (d) 10 stretching-releasing cycles.

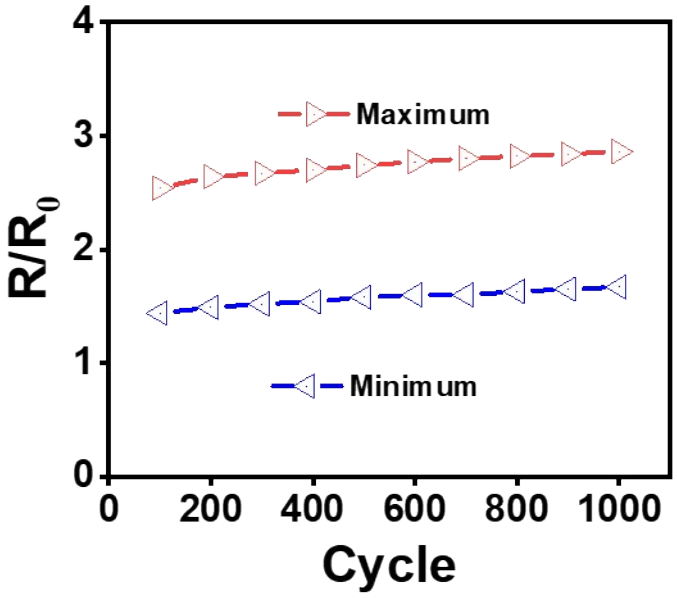

Fig. S25. The maximum and minimum R/R_0 values in different stretching-releasing cycles (1st, 100th, 200th, 300th, 400th, 500th … and 1000th).

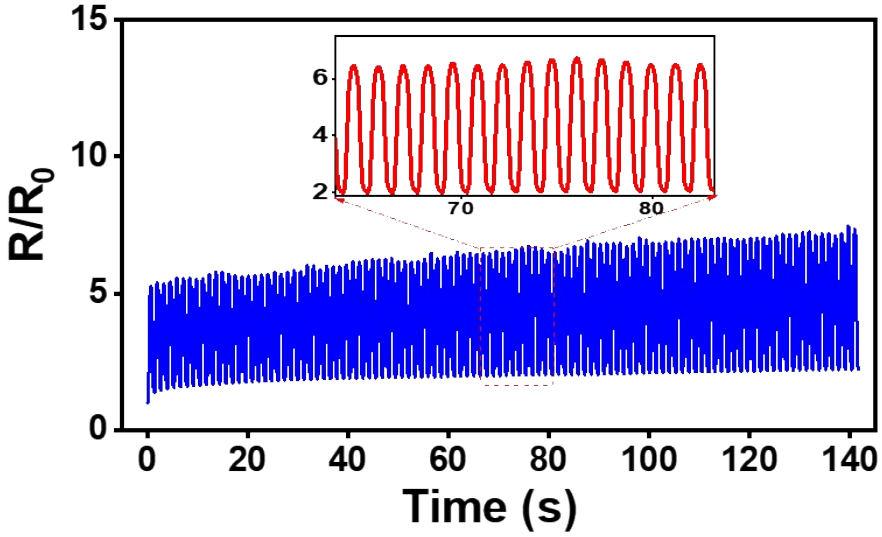

Fig. S26 R/R_0 values of TAMF with 20% strain at a rate of 1000mm/min during 100 stretching-releasing cycles, the insert shows the randomly selected 15 stretching-releasing cycles.

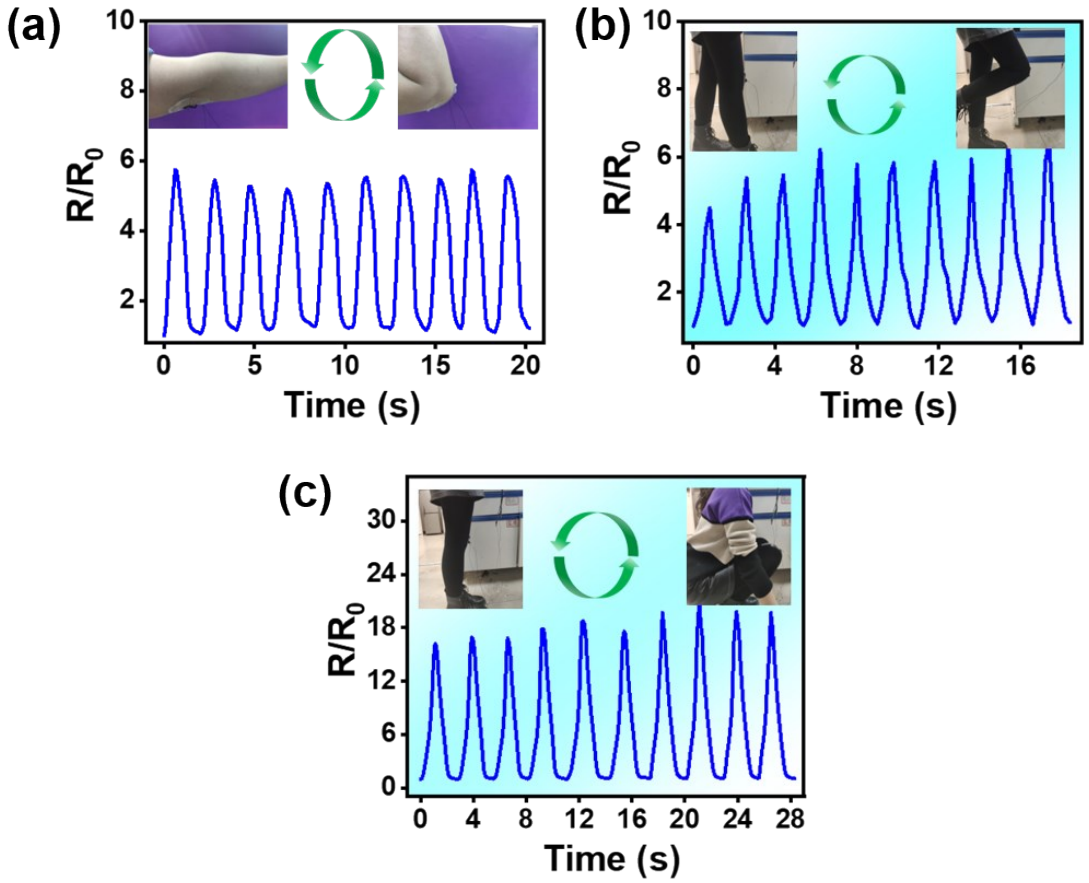

Fig.R27 Real-time relative resistance change to detect elbow bending with varying angle of 30 °, 45 ° and 90 ° (a); real-time relative resistance change to minor the stepping (b) and squatting (c) of a volunteer.

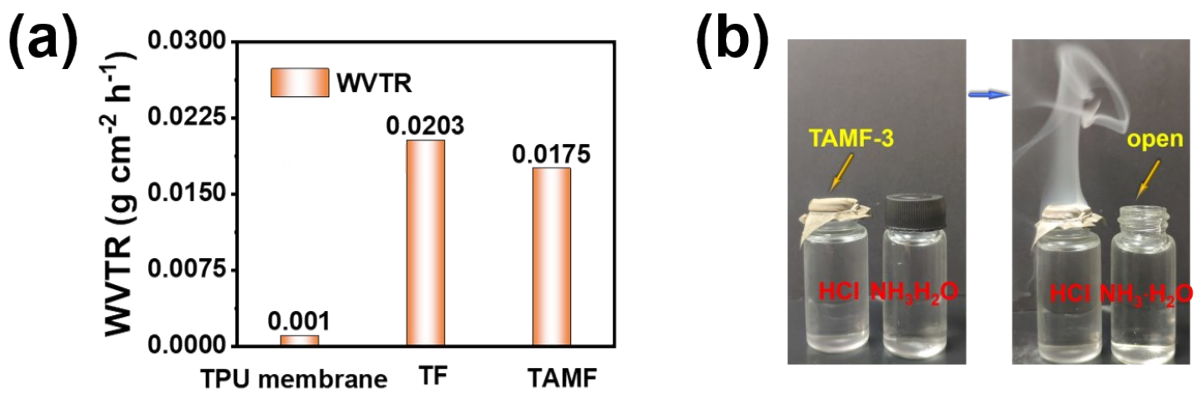

Fig. S28. (a) The WVTR of neat commercial TPU membrane, TF and TAMF film , (b) air permeability of TAMF.

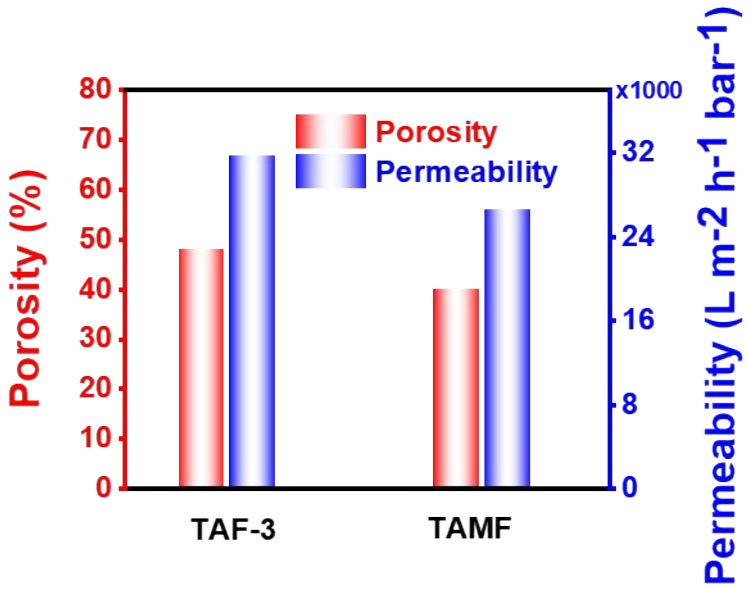

Fig.S29 Porosity and permeability of TAF-3 and TAMF.

References

[1] B. Zhou, Z. Zhang, Y. Li, G. Han, Y. Feng, B. Wang, D. Zhang, J. Ma and C. Liu, *ACS Appl. Mater. Interfaces*, 2020, **12**, 4895-4905.

[2] L. C. Jia, K. Q. Ding, R. J. Ma, H. L. Wang, W. J. Sun, D. X. Yan, B. Li and Z. M. Li, *Adv. Mater. Technol.*, 2019, **4**, 1800503.

[3] J. Liu, H. B. Zhang, R. Sun, Y. Liu, Z. Liu, A. Zhou and Z. Z. Yu, *Adv Mater*, 2017, **29,** 1702367.

[4] Y. J. Wan, P. L. Zhu, S. H. Yu, R. Sun, C. P. Wong and W. H. Liao, *Small*, 2018, **14**, 1800534.

[5] J. Liu, Z. Liu, H. B. Zhang, W. Chen, Z. Zhao, Q. W. Wang and Z. Z. Yu, *Adv Electron Mater*, 2019, **6**, 1901094.

[6] L. Wu, L. Wang, Z. Guo, J. Luo, H. Xue and J. Gao, *ACS Appl. Mater. Interfaces*, 2019, **11**, 34338-34347.

[7] Q.-W. Wang, H.-B. Zhang, J. Liu, S. Zhao, X. Xie, L. Liu, R. Yang, N. Koratkar and Z. Z. Yu, *Adv Funct Mater*, 2019, **29**, 1806819.

[8] Z. Fan, D. Wang, Y. Yuan, Y. Wang, Z. Cheng, Y. Liu and Z. Xie, *Chem. Eng. J*, 2020, **381**, 122696.